ELSEVIER

Coupling dynamical and collisional evolution of small bodies: an application to the early ejection of planetesimals from the Jupiter–Saturn region

Sébastien Charnoz [a,*] and Alessandro Morbidelli [b]

[a] *Equipe Gamma-Gravitation, Université Paris 7 & CEA Saclay, Centre de l'Orme les Merisiers, bat. 709, 91191 Gif-sur-Yvette cedex, France*
[b] *Observatoire de Nice-Côte d'Azur, France*

Abstract

We present a new algorithm designed to compute the collisional erosion of a population of small bodies undergoing a complex and rapid dynamical evolution induced by strong gravitational perturbations. Usual particle-in-a-box models have been extensively and successfully used to study the evolution of asteroids or KBOs. However, they cannot track the evolution of small bodies in rapid dynamical evolution, due to their oversimplified description of the dynamics. Our code is based on both (1) a direct simulation of the dynamical evolution which is used to compute local encounter rates and (2) a classical fragmentation model. Such a code may be used to track the erosional evolution of the planetesimal disk under the action of newly formed giant-planets, a passing star or a population of massive planetary-embryos. We present here an application to a problem related to the formation of the Oort cloud. The usually accepted formation scenario is that planetesimals, originally formed in the giant planet region, have been transported to the Oort cloud by gravitational scattering. However, it has been suggested that, during the initial transport phase, the mutual large encounter velocities might have induced a rapid and intense collisional evolution of the planetesimal population, potentially causing a significant reduction of the Oort cloud formation process. This mechanism is explored with our new algorithm. Because the advantages of our new approach are better highlighted for a population undergoing a violent dynamical evolution, we concentrate in this paper on the planetesimals originally in the Jupiter–Saturn region, although it is known that they are only minor contributors to the final Oort cloud population. A wide range of parameters is explored (mass of the particle disk, initial size-distribution, material strength): depending upon the assumed parameter values, we find that from 15 to 90% of the mass contained in bodies larger than 1 km survives the collisional process; for our preferred choice of the parameters this fraction is $\sim 70\%$. It is also found that the majority of planetesimals larger than 1–10 km are pristine, and not fragments. We show also that collisional damping may not prevent planetesimals from being ejected to the outer Solar System. Thus, although the collisional activity is high during the scattering by Jupiter and Saturn, collisional grinding does not lower by orders of magnitude the mass contained in bodies larger than 1 km, originally in the Jupiter–Saturn region. These conclusions seem to support the classical collisionless scenario of Oort cloud formation, at least for the Jupiter–Saturn region.
© 2003 Elsevier Inc. All rights reserved.

Keywords: Formation of the Solar System; Comets; Collisions; Giant planets; Numerical simulation

1. Introduction

In the current architecture of the Solar System, the populations of small bodies—the asteroid belt, the Kuiper belt and the Oort cloud—lead a quiet life with dynamical evolution timescales comparable or larger than the age of the Solar System. For this reason the current collisional evolution of these populations can be studied with Particle-In-A-Box codes which include only simple models of dynamical evolution (see, for example, Marzari et al., 1995) or no dynamics at all (eccentricities and inclinations are kept constant like in Davis and Farinella, 1997). However, their peculiar orbital distributions indicate that these populations have experienced phases of violent dynamical excitation during the primordial ages of the Solar System, when giant-planet (and possibly other massive bodies) appeared. As soon as

* Corresponding author.
 E-mail addresses: charnoz@cea.fr (S. Charnoz), morby@obs-nice.fr (A. Morbidelli).

the gravitational scattering exerted by the planets emplaced bodies on very eccentric and inclined orbits, some intense collisional process was triggered in the small body populations.

The importance of the collisional activity in the Oort cloud formation process has been recently stressed by Stern and Weissman, 2001 (SW01 hereafter). On the basis of analytical considerations and statistical simulations, SW01 pointed out that bodies initially in the giant-planets region would have suffered a rapid collisional erosion on a timescale shorter than the typical ejection timescale due to giant-planet perturbations. Possible implications of such a mechanism are of great importance:

 (i) the vast majority of bodies in the Oort cloud would be collisionally evolved;
 (ii) collisional disruption would have reduced by a factor 10 to 1000 the contribution to the Oort cloud formation of the giant planet region up to Neptune's distance (the factor of 1000 is deduced from SW01's Fig. 2 in which the half-life of planetesimals is roughly 10 times smaller than the dynamical-ejection timescale, so one may expect a crude 2^{10} factor of reduction before ejection);
 (iii) collisions would have damped eccentricities and inclinations of planetesimals up to the epoch when the disk became sufficiently depleted.

These conclusions, which potentially cast doubts on the classical scenario of Oort cloud formation (see Duncan et al., 1987), were based on Particle-In-A-Box models of collisional evolution, which cannot account for the dynamical evolution induced by the giant-planets and its feedback on the collisional evolution. Consequently there is a need for "a general repraisal of Oort cloud formation models using coupled collisional-dynamical simulations" (SW01).

Developing the appropriate tools for this kind of simulation is precisely the motivation of this work. In the following, we first present an algorithm that allows the self-consistent coupling of both

(1) the dynamical evolution of planetesimals under giant-planet perturbations, and
(2) erosion and fragmentation processes.

Collective effects among planetesimals, like gravitational or collisional stirring and/or damping, cannot be included for the moment, but one may expect them to be very weak due to the low individual-masses of planetesimals compared to giant-planets.

As an application of the new algorithm, in Section 3 we study the collisional evolution of the planetesimals originally in the Jupiter–Saturn region, under a variety of assumptions concerning the mass of the particle disk, the initial size-distribution, and the material impact strength. It is thought that most of the current Oort cloud population originated

from the Uranus–Neptune region. Nevertheless we concentrate on the bodies in the Jupiter–Saturn region because they have the fastest collisional and dynamical evolution, which better illustrates the advantages of our approach over the classic Particle-In-A-Box approach. A more detailed and appropriate study of the formation of the Oort cloud, that accounts also for the population in the Uranus–Neptune region and beyond, will be the subject of a forthcoming paper.

2. Description of the model

2.1. General overview

Our purpose is to compute the time evolution of the size-distribution of a population of small bodies (e.g., planetesimals) evolving under the gravitational influence of some massive bodies (e.g., planets).

Usual collisional evolution codes are based on a statistical approach in which bodies are distributed into multiple batches, according to their mass and sometime also to their semi-major axis (Davis et al., 1989, 1997; Stern and Colwell, 1997). Each batch contains the number of bodies within the batch's range of size and semi-major axes, as well as the mean eccentricity and the mean inclination of these bodies. Collision rates and encounter velocities between all pairs of batches are computed analytically, assuming an a-priori distribution of orbital elements of bodies within each batch. Several analytical tools exist to compute those quantities, depending on some specific approximations. For example, the popular Particle-In-A-Box (PIAB) approach based on kinetic theory of gases is widely used for planetesimal accretion (Greenberg et al., 1978; Spaute et al., 1991). It is usually valid for low eccentricities and inclinations ($\ll 0.1$). More refined methods coming from the study of asteroids are also available (Wetherill, 1967), but assume axisymetric distributions of orbits. The fact that particles are distributed in batches with pre-defined distributions of orbital elements (only the means of distributions are allowed to evolve, at most), prevents the possibility of taking into account the effects of the ongoing dynamical evolution. Such models are powerful tools to study the collisional evolution of a population that is dynamically in steady-state or slowly evolving (like in the current asteroid belt, in the Edgeworth–Kuiper belt or during planetesimal accretion). However, the over-simplified description of the dynamics prevents such codes from being used in dynamically complex and rapidly evolving situations, like that of a population of planetesimals scattered to high eccentricity orbits by planets.

The new approach we present here allows us to couple the collisional evolution with the complex dynamical evolution, without considering any a-priori distribution of orbital elements of planetesimals. It is based on

(1) a direct dynamical simulation of test particles orbiting in the field of the planets (orbits of particles are accurately computed in order to derive local encounter rates) and

(2) a statistical erosion/fragmentation model that evolves the size-distribution of bodies.

The two parts of the algorithm are the following:

1. The first direct simulation is run with a large number of particles orbiting the Sun and undergoing the gravitational perturbations exerted by the planets. It is called the "Reference Simulation hereafter." Particles of the reference simulation are called "Reference Particles" to distinguish them from real planetesimals in the early Solar System. Encounters within some threshold distance between reference particles are detected and the time of the encounter, the encounter velocity and the particles' identification numbers are recorded into an encounter file. The encounter file will be used to compute collision rates and the evolution of the size-distribution of planetesimals. The reference simulation is performed with the code described in Charnoz et al. (2001), a generalization of a Bulirsh–Stoer integrator, modified to efficiently detect close-encounters between particles in weakly collisional systems.

2. To compute the evolution of the size-distribution of planetesimals, each reference particle represents a cloud of planetesimals, characterized by a size-distribution. A size-distribution vector is attributed to each reference particle, containing the number of planetesimals in logarithmic mass-bins. Planetesimals are assumed to have exactly the same orbit as their reference particle. Once all size-distribution vectors have been initialized (depending on the total mass of the system and the initial size-distribution of planetesimals), encounters are read in the encounter file in chronological order: as two reference particles encounter each other, the evolution of the size-distribution of the two planetesimal clouds, encountering each other with the recorded relative speed, is computed with a standard fragmentation model (see Section 2.3). The number of collisions between each pair of size-bins is computed by normalizing the number of encounters of reference particles by the cross-section of the planetesimals (see Section 2.2).

The size-distribution associated with every reference particle evolves collision after collision. At the end of the run, the global size-distribution of the whole system is obtained by summing bin-per-bin the size-distribution of all reference particles. One advantage of this hybrid method is the possibility to determine the size-distribution of planetesimals in any specific dynamical situation (i.e., on inclined orbits, in the Lagrangian points of giant planets...). One just has to select the reference particles in the desired dynamical configuration, and sum bin-per-bin the size-distributions that they represent.

In the spirit of fluid-dynamics, our approach may be qualified as Lagrangian, since particles are individually followed and local properties are computed by doing some statistics on closest neighbors. Conversely, the classical methods follow a more Eulerian approach: usually the number of particles entering and leaving the population is computed for each box of a grid, and the relevant quantities (like random velocities, orbital elements, etc.) are evolved with time according to some model (see, for example, Kenyon and Luu, 1999; Stern and Colwell, 1997; Spaute et al., 1991). The only (and major) constraint of our Lagrangian approach is that the dynamics of reference particles must be the same as those of planetesimals. In other words, the orbits of planetesimals are assumed to be entirely controlled by the giant planets' perturbations. Thus dynamical effects induced by collisions between planetesimals are not included: collisions and encounters among planetesimals are assumed not to affect the dynamical evolution. The latter assumptions are usual in collisional evolution models (Davis et al., 1989, 1997). Gravitational enhancement of planetesimal's cross-section is not considered since encounter velocities are typically very high ($\geqslant 10^3$ m/s).

2.2. Collision rate among bodies

2.2.1. Collision rate scalings

We derive here the scaling rule by which we compute the number of collisions between planetesimals when two reference particles have an encounter. Let R_{ref} be the maximal half-distance for which encounters are recorded in the encounter file (1.5×10^{-3} AU). During a time ΔT, on average the number of encounters between two given reference particles i and j is $N_E(i, j)$ (considering one target and one projectile):

$$N_E(i, j) = P_{i,j} \times \pi (R_{ref} + R_{ref})^2 \times \Delta T. \qquad (1)$$

Where $P_{i,j}$ is the intrinsic collision rate per unit time and per unit cross-sectional area of particles i and j, and $\pi (R_{ref} + R_{ref})^2$ is their combined cross-section. We turn now to the scaling rule for planetesimals. Let R_l be the effective radius of planetesimals in mass-bin number l. Let $N(j_l)$ be the number of particles in the l mass bin represented by reference particle j. Initially $N(j_l)$ is simply the total number of planetesimals with size R_l in the system, divided by the number of reference particles. We also introduce $N_C(i_k, j_l)$, the number of collisions suffered by one planetesimal in size-bin k of reference particle i with all planetesimals in size-bin l of the reference particle j during the same time interval ΔT as in (1). Planetesimals are assumed to have the same orbit as their corresponding reference particles (see Section 2.1), so that the intrinsic collision rate per unit time and per unit cross-sectional area ($P_{i,j}$) for planetesimals is the same as for the reference particles. Following (1):

$$N_C(i_k, j_l) = N(j_l) \times P_{i,j} \times \pi (R_k + R_l)^2 \times \Delta T. \qquad (2)$$

The link between (1) and (2) is performed by considering that when one encounter is recorded between reference particles i and j the number of collisions $N_E(i, j)$ equals 1. This yields:

$$P_{i,j} = \frac{1}{\pi (R_{ref} + R_{ref})^2 \times \Delta T}. \tag{3}$$

Then comes the scaling rule:

$$N_C(i_k, j_l) = \frac{N(j_l)(R_k + R_l)^2}{4R_{ref}^2}. \tag{4}$$

Equation (4) simply states that the number of collisions among planetesimals is proportional to the number of encounters between reference particles, the scaling factor being simply the ratio of the cross-sections times the number of projectile bodies (we remind the reader that (4) is established for $N_E(i, j) = 1$). This is basic result of the kinetic theory of gases. One may note that rigorously $N_E(i, j)$ (or $N_C(i_k, j_l)$) is a random variable with mean value given by (1) or (4). Here, it is implicitly assumed that the time of the first collision equals the average collision time, which is of course false since collision-times follow in general a Poisson's distribution. Over many collisions, this effect is correct because the mean value of the encounter times tends toward the average encounter time. On the other hand, we believe that counting encounters in the reference simulation gives a better estimate of the real collision probability than applying the standard Öpik formulae (see Wetherill, 1967) using the reference particles' orbital elements at discrete timesteps. In fact, the Öpik formulae average over the angular phases (mean anomaly, longitude of node, argument of perihelion) assuming that semimajor-axes, eccentricities, and inclinations are roughly constant. But in the case of a dynamics dominated by the scattering action of the giant planets, the variations of a, e, i occur on a much shorter timescale than the precession of the secular angles, partially invalidating Öpik's procedure.

Reference particles i and j are treated symmetrically for the evolution of their mass-distribution. They are considered first as target-projectile respectively and afterwards as projectile-target. Once both mass-distributions have been evolved (see Section 2.3), the next encounter is read in the encounter file and the size-distributions held by the two new colliding reference particles are evolved and so on.

2.2.2. Numerical implementation

Despite the apparent simplicity of the computation of the number of collisions in (4), a rather more complicated scheme must be applied to ensure numerical accuracy and self-consistency. We describe these aspects here. The mass-distribution held by the target reference particle i is evolved by considering each pair of mass-bins (k, l) separately. However, in order to prevent a too-fast evolution (not appropriate for an accurate computation), the total number of destructive collisions, suffered by one target planetesimal, must be evaluated *before* processing the fragmentation process. The number of destructive collisions suffered by one target planetesimal in mass bin k (held by the reference particle i) with all incoming planetesimals held by the reference particle j, is $N_C(i_k)$:

$$N_C(i_k) = \sum_l N_C(i_k, j_l) \tag{5}$$

in which the sum is performed over those mass-bins l which are massive enough to destroy or erode planetesimals in mass-bin k. Usually, $N_C(i_k) < 1$ and only the fraction $N_C(i_k)$ of planetesimals in mass-bin k will receive a collision, others remaining unaffected. For numerical accuracy, the number of destroyed planetesimals must be small compared to the total number of target planetesimals. For example, an obvious critical situation is when $N_C(i_k) > 1$, which means more than one destructive collision per planetesimal. To avoid this, the following scheme is applied: Remember that $N_C(i_k)$ is the number of collisions happening in a time interval ΔT. We introduce the dimensionless quantity $t' = t/\Delta T$, with t standing for time. Evolving the size-distribution over a time period ΔT is equivalent to going from $t' = 0$ to $t' = 1$ with small time-steps dt'. During a time step dt', the number of collisions is $N_C(i_k) \times dt'$, assuming a constant intrinsic collision probability inside the time-interval ΔT. At the beginning of a time-step, $N_C(i_k)$ is evaluated for all values of k, with the distribution resulting from the previous step. Then, a new time-step dt' is chosen such that less than 20% of planetesimals are destroyed in all mass-bins k during the step. The size-distributions are evolved and t' is incremented by dt'. The process ends when $t' = 1$. This method ensures a slow and self-consistent evolution of size-distributions to preserve numerical accuracy. It is the same as in classical codes of collisional-evolution in which the intrinsic collision probability is kept constant and where size-distributions are evolved iteratively with a small time-step. Note that our scheme does not require explicit knowledge of ΔT. The choice of dt' is, of course, arbitrary. Linking dt' to the threshold of 20% destruction is the result of a compromise between accuracy and computing time. We have done tests with dt' imposed by a more restrictive threshold (such that only 1% of the population is destructed in the timestep dt'), and checked that the differences in the final distributions are of order of a few percent for the smallest bodies and less than 1% for kilometer-size bodies.

2.3. Fragmentation model

2.3.1. Outcome of collisions

A simple fragmentation model was adopted because the physics of fragmentation is poorly known as are the physical parameters of planetesimals. This also makes the interpretation of results easier. Following Marzari et al. (1995) and Petit and Farinella (1993), when a target planetesimal (with mass M_t) is hit by a projectile the ratio f between the mass

of the largest fragment and that of the target body is calculated according to a simple empirical law (Fujiwara et al., 1977):

$$f = 0.5 \left(\frac{SM_t}{\rho 0.5 E_{\text{rel}}} \right)^{1.24}. \tag{6}$$

In (6), ρ is the material density, S is the impact strength (i.e., the energy per unit volume for shattering 50% of the mass of the parent body) and E_{rel} is the kinetic energy in the barycentric reference frame. The value of S is discussed in Section 3.1.2.

Two fragmentation regimes are considered:

1. If $f \leqslant 0.5$ fragmentation is catastrophic. A size-distribution of fragments is generated and distributed into bins of smaller size, such that $dn \propto m^{-p} dm$ with $p = 1/(1 + f)$, consistent with conservation of the target's mass. These fragments are added to the size-distribution of the parent body's reference particle. The parent body is then removed from the size-distribution.

2. If $f > 0.5$ there is cratering. The new mass of the target body is $f \times M_t$ and the total mass of crushed material is $(1 - f) \times M_t$, where the largest fragment has a mass of $(1 - f) \times 0.2 M_t$ and with a size-distribution of fragments with $dn \propto r^{-3.5} dr$. It is added to the size-distribution held by the target's reference particle. The 0.2 factor is taken from the cratering model of Wetherill and Stewart (1993). The total mass of crushed material is removed from the mass-bin of the parent body. Fractional numbers of bodies in the size-distributions are allowed to ensure mass-conservation. Mass-conservation is enforced after every fragmentation by multiplying the number of fragments generated in all mass-bins by a normalization factor so that the total-mass of fragments numerically matches the analytical computation (down to the lower cut-off).

This cratering model is taken from Wetherill and Stewart (1993) and Kenyon and Luu (1999), but in our case it does not include gravitational reaccumulation. This choice is appropriate for the cases where the impact velocity is much larger than the escape velocity of planetesimals, which prevents substantial reaccumulation of material. It is possible, however, to adopt impact-strength scaling-laws in which reaccumulation is implicitly taken into account in the form of an enhanced value for S (as in our cases C5-1 to C5-4 in Section 3).

2.3.2. Lower cutoff of size-distribution

Campo-Bagatin et al. (1994) has shown that sampling a size-distribution into discrete size-bins with a lower mass cut-off introduces an artificial discontinuity into the size-distribution, triggering a wave that propagates from smaller sizes up the largest sizes. To cancel this artifact, the following scheme is applied: among the 65 mass-bins that we use in our algorithm, the 25 first bins (numbered 1 to 25, with sizes ranging from 1 mm to 20 cm) are considered as "dust bins":
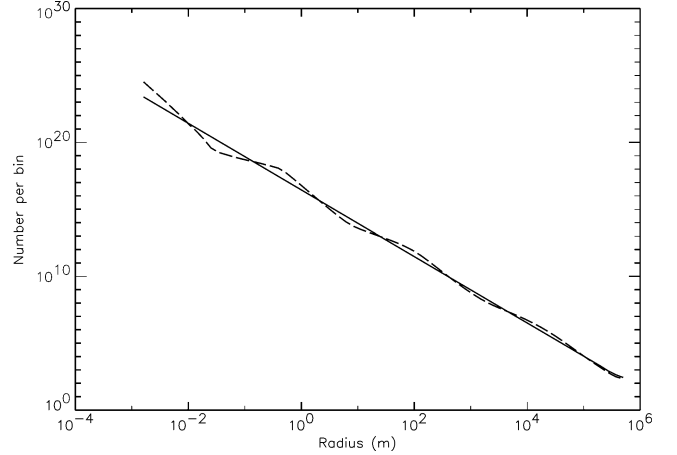

Fig. 1. Resulting cumulative size-distributions obtained without cut-off-correction (dashed line, notice the wavy structure) and with cut-off-correction (solid line).

the number of bodies they contain is not self-consistently computed like for the other bins, but extrapolated using a simple power-law on the basis of the 5 next bins (numbered from 26 to 30). This scheme is very efficient and cancels completely the artificially wavy structure (see Fig. 1). A similar scheme was used in (Marzari et al., 1997) for the study of Trojan Asteroids. The validity of this method relies on the size-independency of the fragmentation model, in particular on a constant value for the impact strength S with size (Campo-Bagatin et al., 1994).

We have performed multiple tests, which all reproduce the classical result according to which the differential size-distribution ($dN/dr \propto r^q$) tends toward a power law with exponent -3.5 in the case of a size independent fragmentation model (Dohnanyi, 1969; Paolicchi, 1994; Tanaka et al., 1996), whatever the initial size-distribution. For examples, starting with distributions with $q = -3, -3.5, -4.1$, the final distributions have slope indices $q = -3.486, -3.506, -3.485$, respectively, in close agreement with theoretical results.

3. Example: application to the planetesimals in the Jupiter–Saturn zone

3.1. Model parameters

As explained in the previous section, the parameters of the model that must be set at the beginning of the simulation are:

- For the reference simulation: the total number of particles (N_{ref}), the threshold half-distance used to record close encounters (R_{ref}) and their initial positions and velocities.
- For the Collisional Evolution Simulation: the initial size-distribution vectors for every reference particle, the impact strength (S), their internal density (ρ).

Below, we detail on the values assumed for these parameters for the various cases that we have examined.

3.1.1. Parameters of the reference simulation

Reference particles are spread between Jupiter and Saturn, with eccentricities and inclinations of 0.001 and 0.0005, respectively, and with a uniform semi-major axis distribution to sample with uniform density all the radial extent of the system. Jupiter and Saturn are introduced at the beginning of the simulation with their present masses and with their orbital elements relative to the invariable plane (Nobili et al., 1989). The total number of particles (N_{ref}) and the threshold value for close encounters (R_{ref}) should be chosen such that the collision frequency in the reference simulation is high enough to sample with accuracy the evolution of collision rate during the phase of ejection and the distribution of impact velocities. Values of 10,000 for N_{ref} and 5×10^{-4} AU for R_{ref} were chosen. The typical collision time in the reference simulation is about 1000 years, well below dynamical and collisional timescales (for bodies larger than 1 km), ensuring a good sampling. The values adopted for all parameters are summarized in Table 1. The reference simulation was done for 1.3×10^5 years to cover the typical ejection timescale, which is about 4×10^4 years (Holman and Wisdom, 1993). A total of 122,000 encounters was recorded, i.e., about 25 encounters per particle (because each encounter involves two particles).

The encounter distance R_{ref} introduces an artificial increase of encounter velocities, ΔV, due to Keplerian shearing. This effect is often encountered when studying dense collisional systems like planetary rings. Brahic (1976) and Hertzsch et al. (1997) give:

$$\Delta V = R_{ref} \times \Omega_K \tag{7}$$

where Ω_K is the local Keplerian frequency. With our choice of R_{ref}, $\Delta V = 5$ m/s at 5 AU and less than 1 m/s beyond 9 AU, which is negligible compared to the 10^3 to 10^4 m/s relative velocities induced by Jupiter and Saturn.

Table 1
Parameters of the model

Reference simulation	
Number of particles (N_{ref})	10000
Threshold half-distance for recording encounters (R_{ref})	1.5×10^{-3} AU
Collisional evolution simulation	
Number of mass bins	65
Min–max radii	1 mm to 500 km
Range of dust bins	1 mm to 0.2 m
Impact strength (S)	3×10^6 erg/cm^3 for cases C1- and C2-
	10^5 erg/cm^3 for cases C3-
	strain-rate model for cases C4-
	hydrocode model for cases C5-

3.1.2. Parameters of the collisional evolution simulation constant parameters

The mass distributions are discretized over 65 logarithmic bins, with a constant 2.5 mass ratio between adjacent bins. Masses range from 1.7×10^{-5} to 5×10^{20} kg. Each bin contains the number of planetesimals in the bin's mass range. Non-integer numbers of planetesimals are allowed in order to ensure mass conservation during cratering processes. Fractional numbers are interpreted as an existence probability when the number of collisions among planetesimals is computed. All the planetesimals in a mass-bin have the same effective mass, equals to the geometric-mean of the bin's mass-range. The planetesimals' effective radius is computed by assuming spherical shape and a density of 1 g/cm^3. Due to this direct equivalence, the mass-distribution is sometime called size-distribution in the following. The sizes of the objects in the bins of largest and smallest mass are 1 mm and 500 km, respectively.

Impact strength. The impact strength, S, of primordial planetesimals is unknown. Impact experiments (Ryan et al., 1991, 1999) reveal that the impact strength of fractured or porous ice is comparable to solid ice because the impact energy is not transmitted by the void spaces inside the bodies. Following Davis and Farinella (1997); value of $S = 3 \times 10^6$ erg/cm^3 is considered, in agreement with Ryan et al. (1999) for crushed icy bodies. The impact strength is kept constant over size in the standard version of our collisional model, for self-consistency with the lower-cutoff extrapolation method (see Section 2.3.2) and for a clearer interpretation of results. This choice is also consistent with the conclusions of Colwell et al. (2000) who, for outer planets' satellites, found only a weak dependence of S on the size of the impact body. To explore the influence of S, it was also lowered to 10^5 erg/cm^3 in some simulations. We also ran two other sets of simulations with S varying with size according to

(1) a classical strain-rate scaling law (Housen et al., 1991) taking $S = 3 \times 10^6$ erg/cm^3 for 10 cm bodies, and
(2) a modern 3D Hydrocode law proposed by Benz and Asphaug (1999) for ice at 3 km/s impact velocity.

Note that in the strain-rate model, the weakest bodies are kilometer-sized, while in the hydrocode model they are 100 m sized, which will have important consequences on the size-evolution of bodies (see Section 3.3.4). The different models used for the impact strength are shown in Fig. 2.

Initial size-distributions. Because the initial size-distribution of planetesimals is unknown, several initial conditions are considered here, based on the current knowledge of collisional and accretional processes. On the one hand, several authors (for example, Dohnanyi, 1969; Paolicchi, 1994; Tanaka et al., 1996) have shown that fragmentation among a population of bodies with different sizes lead to an equi-
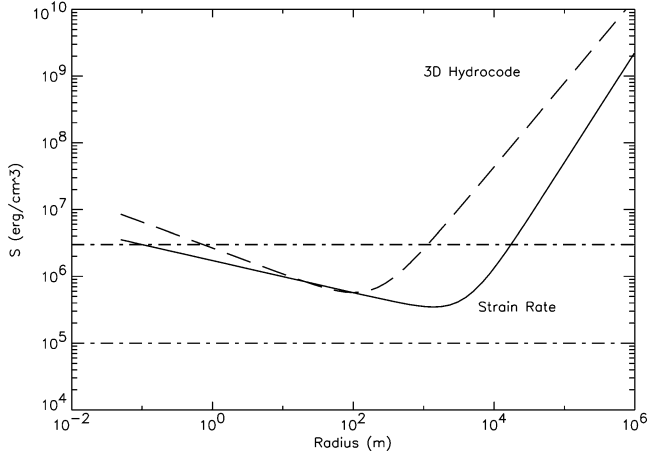
Fig. 2. Scaling laws for the impact strength S of planetesimals. The strain rate model (Housen et al., 1991) is displayed with a solid line and the hydrocode scaling law (Benz and Asphaug, 1999) is displayed with a dashed line. Constant values of S are also displayed (with dashed dotted lines) for comparison.

librium differential size-distribution with a power law index $q = -3.5$, if the fragmentation process is size independent. On the other hand, if Runaway Growth was an effective mechanisms among the most massive planetesimals ($\geqslant 1$ km), the resulting size-distribution may have been initially very steep, as observed in Runaway Growth simulations (Wetherill and Stewart, 1989, 1993; Spaute et al., 1991). Wetherill and Stewart (1993) find that planetesimal accretion results in a bimodal size-distribution, with a fragmentation-tail (< 1 km) with $q \sim -3.5$, and an accretion-tail ($\geqslant 1$ km) with $q \sim -5.5$. Two cases will be considered here

(1) a single power law size-distribution with $q = -3.6$, and
(2) a bi-modal size-distribution with $q = -3.5$ for bodies smaller than 1 kilometer and $q = -5.5$ for larger bodies.

The total mass of planetesimals between Jupiter and Saturn is also an unknown parameter as it relates to the initial mass of the protoplanetary nebula, consequently three cases will be considered here: 6.5, 11.5, and $50M_\oplus$, equivalent to 0.6, 1, and 5 times the minimum-mass nebula (in addition to the giant-planets' masses). The $11.5M_\oplus$ disk is our standard case. The last parameter that determines the initial size-distribution is the size of the largest body. Observations show that cometary nuclei are typically kilometer-size and comet Hale–Bopp is thought to have a radius of 20–40 km. Kuiper-belt objects are also good primitive object candidates, with a maximum size of several 100 km in radius. Stern (1991) argues for the existence of a primordial population of 10^3 km bodies in the outer Solar System. Thus the biggest planetesimals could be roughly in the range 50 to 500 km diameter. Both cases will be considered. Once the initial mass distribution is set-up for the whole system, it is equally distributed among the size-distribution vectors corresponding to each reference particle. Thus each mass bin of

each vector contains exactly $1/N_{\mathrm{ref}}$ times the total number of bodies of corresponding mass.

In summary, a total of 12 different initial size-distributions will be considered by varying 3 parameters:

(1) the slope q of the size-distribution;
(2) the size of the biggest planetesimal $R_{\max}$ at which the size distribution is truncated; and
(3) the total mass M of material between Jupiter and Saturn.

Another set of 12 simulations was also performed with different models for the impact strength. All cases are summarized in Table 2.

3.2. Dynamics of ejection

We first present the results of the reference simulation, to discuss the process of scattering of planetesimals towards the outer Solar System from a purely dynamical point of view. Because of the presence of Jupiter and Saturn (introduced at the very beginning of the integration), particles' eccentricities and inclinations are rapidly increased (Fig. 3). However, eccentricities are raised even more rapidly than inclinations (a 100 year timescale compared to a few 1000 years for inclinations) due to the low inclination of the giant planets (< 0.02 radians). Thus, the common assumption $i = e/2$, valid for a dynamical equilibrium, is strongly incorrect during the first few 1000 years of evolution. During this early period when $e \gg i$, the dynamics of the system becomes almost two-dimensional and the collision rate is raised by a factor roughly $\propto e/i$. This can be seen in Fig. 4 where the collision time (inverse of collision frequency) measured in the reference simulation at different epochs is scaled to the case of 1.5×10^{13} kilometric bodies (representing a total mass $\sim 10M_\oplus$) for practical use.[1]

At $t = 0$, the mean collision time for kilometer-sized bodies is about 5×10^4 years, in good agreement with simple estimates (see SW01) based on the kinetic theory of particles. As soon as the system is excited by Jupiter and Saturn, the asymmetry between e and i increases the collision-rate, so that the collision-time falls to 6×10^3 years. Such collision enhancement due to a high e/i ratio has been observed and described for Jupiter-scattered planetesimals in Charnoz et al. (2001). Beyond 1000 years of evolution, the collision-time increases again (i.e., the collision rate decreases) because of two factors:

1. Inclinations progressively reach equilibrium, and are raised to $i \sim e/2$. In theory, the collision-time may re-

---

[1] In the remainder of the paper, collision times are always given for a disk made of 1 km bodies only (no size-distribution) with total mass equals to the minimum mass nebula between Jupiter and Saturn. This is equivalent to the intrinsic collision probability but gives a more direct appreciation of the timescales at play.

Table 2
Initial conditions and results

Name	Size distribution[a]	Largest planetesimal	Total mass ($M_\oplus$)[b]	Remaining 1 km bodies[c]	Remaining $\geqslant$ 10 km bodies[b]	Limit of > 50% pristine[d]	Number of figure
$S = 3 \times 10^6$ erg/cm^3							
C1-1	power-law	50 km	11.5	75%	80%	3 km	8
C1-2	power-law	500 km	11.5	93%	96%	1 km	8
C1-3	power-law	50 km	50	50%	55%	10 km	
C1-4	power-law	500 km	50	83%	85%	10 km	
C1-5	power-law	50 km	6.5	83%	85%	1 km	
C1-6	power-law	500 km	6.5	95%	97%	300 m	
C2-1	bimodal	50 km	11.5	22%	45–90%	500 m	8
C2-2	bimodal	500 km	11.5	22%	45–100%	500 m	8
C2-3	bimodal	50 km	50	15%	30–80%	300 m	
C2-4	bimodal	500 km	50	15%	30–100%	300 m	
C2-5	bimodal	50 km	6.5	30%	55–90%	500 m	
C2-6	bimodal	500 km	6.5	30%	55–100%	500 m	
$S = 10^5$ erg/cm^3							
C3-1	power-law	50 km	11.5	28%	30%	10 km	9
C3-2	power-law	500 km	11.5	68%	72%	30 km	9
C3-3	bimodal	50 km	11.5	16%	25–38%	70 m	9
C3-4	bimodal	500 km	11.5	16%	25–100%	70 m	9
$S =$ strain-rate model							
C4-1	power-law	50 km	11.5	28%	30–100%	1 km	10
C4-2	power-law	500 km	11.5	70%	72–100%	2 km	10
C4-3	bimodal	50 km	11.5	16%	50–100%	200 m	10
C4-4	bimodal	500 km	11.5	16%	50–100%	200 m	10
$S =$ hydrocode model							
C5-1	power-law	50 km	11.5	68%	95–100%	400 m	11
C5-2	power-law	500 km	11.5	80%	98–100%	200 m	11
C5-3	bimodal	50 km	11.5	35%	90–100%	400 m	11
C5-4	bimodal	500 km	11.5	35%	90–100%	400 m	11

This table summarizes results shown in Figs 8 to 11.

[a] "Power-law" refers to a single $q = -3.6$ differential size-distribution, "bimodal" refers to a distribution with $q = -3.5$ for $r < 1$ km and $q = -5.5$ for $r > 1$ km.

[b] 6.5, 11.5, and $50M_\oplus$ correspond to a disk's mass of 1.6, 2, and 5.3 times the minimum mass nebula between Jupiter and Saturn, respectively (leftover material + planets).

[c] Ratio of the final number to the initial number of bodies in the size range, these bodies may be pristine or fragments.

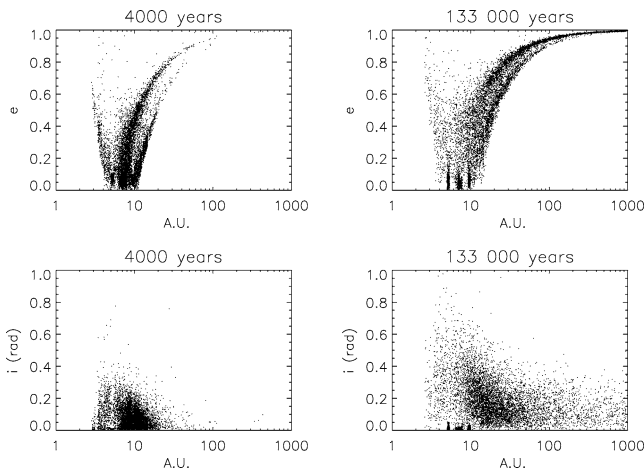[d] Radius above which at least 50% of planetesimals are pristine and not fragments.

Fig. 3. Eccentricity and inclination versus semi-major axis of 10,000 particles in the reference simulation after 4000 and 130,000 years of evolution.
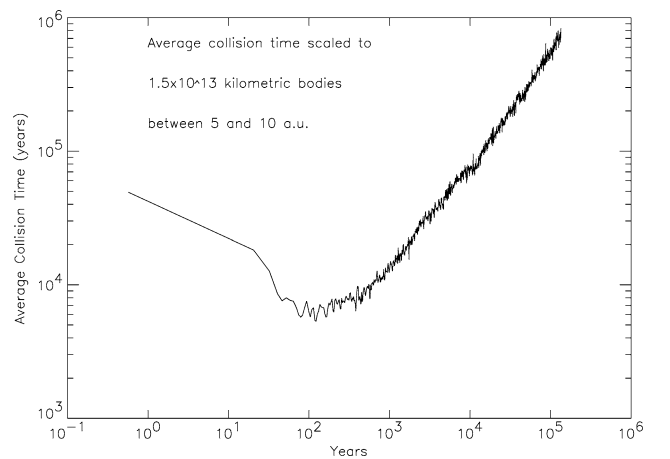

Fig. 4. Collision time (inverse of collision frequency) measured in the reference simulation and scaled to a $10M_\oplus$ population of kilometer sized planetesimals. Each point is computed by averaging more than 100 collisions recorded in the reference simulation.
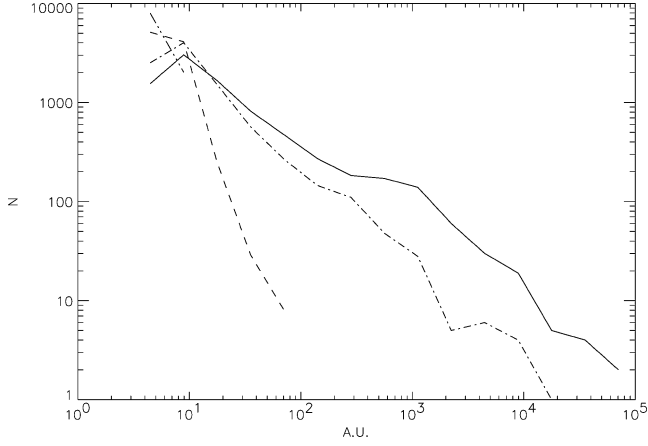
Fig. 5. Distribution of semi-major axes at different epochs: $t = 0$ (dashed double-dots), $t = 4000$ years (dashed line), $t = 50000$ years (dashed-dotted line) and 133,000 years (solid line).

turn to its initial value of 5×10^4 years. However, the collision-time becomes larger than this value because:

2. Particles are progressively transported to larger heliocentric distances and the system is rapidly depleted (see Fig. 5).

The rapid dynamical depletion of the system induces a rapid increase of the collision-time. The number of particles below 10 AU is halved in $\sim 3 \times 10^4$ years, in close agreement with Holman and Wisdom (1993). After 1.3×10^5 years of evolution, only 20% of particles still remain in the Jupiter–Saturn region. The other particles are widely spread, up to the inner edge of the Oort-Cloud and several particles (1121 of 10,000) have been ejected from the Solar System on hyperbolic orbits. The least depleted regions are

(1) in the 1 : 1 resonance with Jupiter;
(2) in the 1 : 1 resonance with Saturn; and
(3) halfway between both planets (Fig. 3).

At this epoch the average collision-time has risen to 10^6 years and increases proportionally to $T^{0.7}$ where T is the time. Thus the main phase of collisional evolution is concentrated in the first 10^4 years of evolution. This is why we did not continue the computation beyond 1.3×10^5 years.

The locations of collisions in the disk are shown in Fig. 6. Although the system spreads to larger heliocentric distances, the great majority of collisions takes place between 5 and 10 AU, and no encounter is detected beyond 20 AU (Fig. 6). A priori, this might be an artifact of having a particle disk initially extending only to 10 AU. However, particles scattered by Jupiter and Saturn are put on inclined orbits, so that they cross a dynamically cold planetesimal disk only where they cross the plane, at the two nodal distances. Figure 7 shows the relative distribution of the nodal distances, cumulated up to 10^5 years (solid) and 1.3×10^6 years (dashed). For each particle, the nodal distances have been recorded once per orbital period. As one sees, most of the nodal distances are
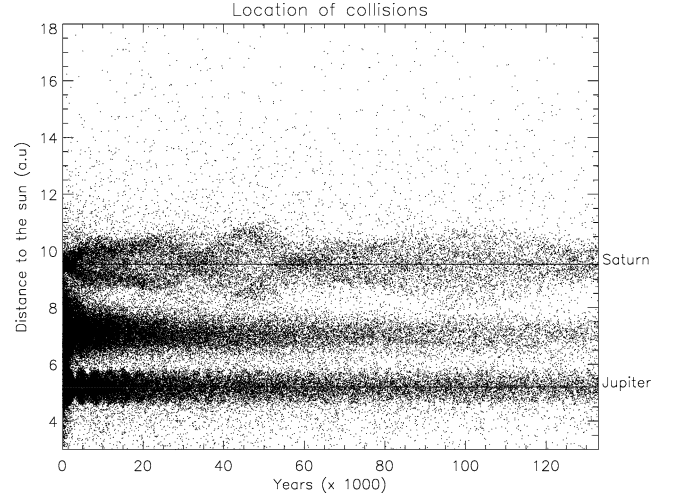

Fig. 6. Location and time of all recorded encounters (122,000 in this plot). The location is the mean heliocentric distance of both encountering reference particles at the instant of their encounter.
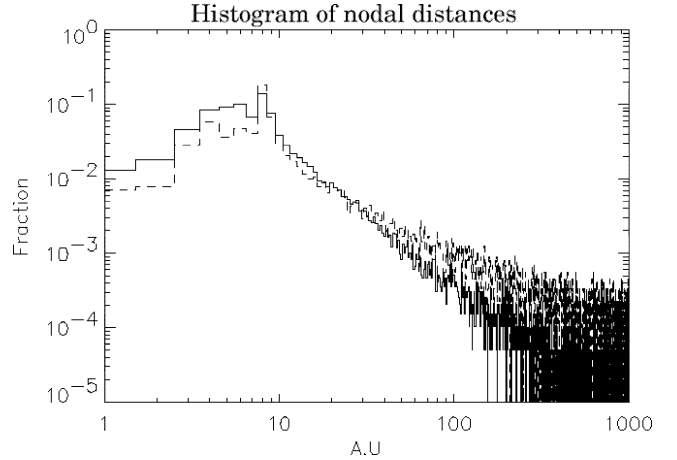

Fig. 7. Histogram of location of nodes location of particles' orbit. For each particle, the two nodal distances has been recorded once per orbital period. Both histograms have been normalized to 1. Thick line: after 10^5 years evolution, dashed-line: after 1.3×10^6 years evolution.

within 11 AU (78% at 10^5 years and 58% at 10^6 years). In addition, when nodal distances are weighted according to the particle orbital-frequency, we find that 95% of the total number of disk-plane-crossing per year occurs within 12 AU in both cases. Then, we think that the consideration of a dynamically cold disk of planetesimals beyond Saturn would not considerably change our result. Further investigation on this point, on longer timescales, will be presented in a future paper on the formation of the Oort cloud, including particles in the trans-saturnian region. We also note that the scattered particles are dispersed along curves of constant perihelion in the (a, e) diagram (Fig. 3). This reflects a close conservation of the Tisserand parameter (which is strictly conserved when only one perturbing planet is present on a circular orbit). Therefore, the scattered particles must all pass at every revolution close to their starting point where the density—and thus the collision probability—is high compared to neigh-

boring regions. As a consequence, collisions take place preferentially in three regions (darker regions in Fig. 6):

(1) close to the orbit of Jupiter;
(2) halfway between Jupiter and Saturn;
(3) close to the orbit of Saturn.

These regions are precisely those where dynamical ejection timescales are the longest and therefore are the most densely populated. This suggests that planetesimals in the Lagrangian Points of Jupiter and Saturn may have suffered an intense collisional evolution under the heavy bombardment of young comets. Since collisions are concentrated around the perihelion of the planetesimals' very elongated orbits, the usual Particle-In-A-Box approximation to compute encounter velocities (of the kind of $\Omega_K a \sqrt{e^2 + i^2}$) would be incorrect. The real collision-velocities are of the order of the orbital-velocities at perihelion, namely from 1 to 10 km/s.

3.3. Collisional evolution

We now discuss the evolution of the size distribution, resulting from the collisional evolution code. In all cases presented below, the size distribution is computed by summing the number of bodies in each of the size-bins associated with the reference particles. Only reference particles scattered by the planets onto orbits with semi-major axes larger than 12 AU are considered (i.e., about 7000 particles). Although only a small fraction of these bodies will be eventually stored in the Oort cloud, we consider that their mass distribution is representative of that of the resulting Oort cloud population coming from the Jupiter–Saturn region. This implicitly assumes that the process that forms the Oort cloud randomly samples the scattered population, and that no subsequent evolution of sizes occurs in the Oort cloud through the age of the Solar System.

All results corresponding to the considered cases are presented in graphic form with 4 panel figures (Figs. 8 to 11) showing:

(a) the initial size-distribution;
(b) the ratio of the final distribution to the initial one (bin per bin) to emphasize evolution;
(c) the time evolution of mass contained in bodies larger than 1 km radius ($M(> 1\ \text{km})$); and
(d) the fraction of "pristine" bodies at the end of the run (i.e., the fraction of bodies which did not suffer any catastrophic fragmentation) for each size's bin.

Several aspects of the results are quantified in Table 2 to make the comparison among the different cases easier.

3.3.1. Standard case: total mass of $11.5 M_\oplus$

The starting size-distribution is that indicated by C1-1 in Table 2: a power law index $q = -3.6$ $R_{\max} = 50$ km, and
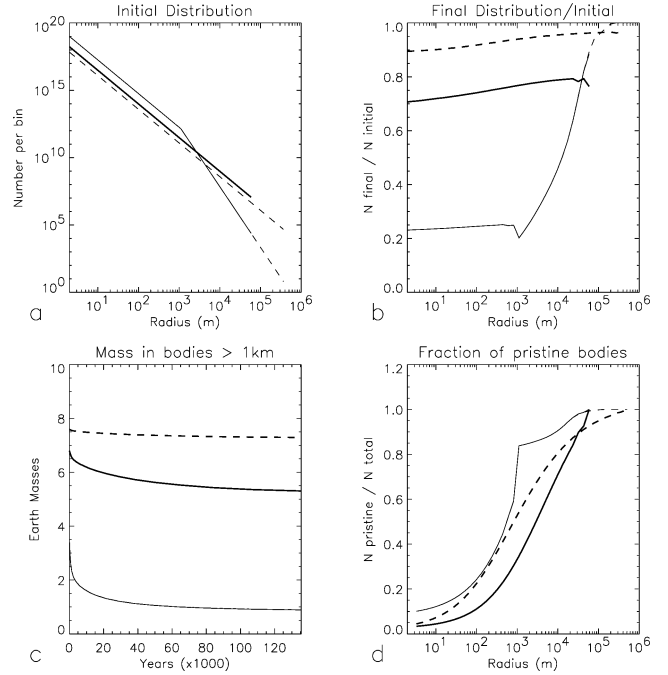

Fig. 8. The total mass of planetesimals is $11.5 M_\oplus$. Collisional evolution for initial size-distribution C1-1 (bold solid), C1-2 (bold dash), C2-1 (solid), C2-2 (dashed) (see Table 2). The starting total mass of planetesimals between Jupiter and Saturn is $11.5 M_\oplus$. (a) Initial size-distribution. (b) Final distribution divided by the initial one, to emphasize variation in the number of bodies. (c) Mass contained in bodies larger than 1 km as a function of time. (d) Fraction of pristine bodies, i.e., fraction of bodies that survived intact throughout the collisional process. Notice that cases C2-1 and C2-2 follow very similar evolutions, resulting in an overlap of the two curves (dash and solid).

total mass of $11.5 M_\oplus$ (Fig. 8a, bold solid line), consistent with a $50 M_\oplus$ total mass of solid material from Jupiter to Neptune, which is roughly the minimum mass nebula (in addition to the giant planets' masses). So the total mass of planets plus the leftover material is about twice the minimum mass nebula. At the end of the run, the number of bodies in each size-bin is about 65–75% of the starting one (Fig. 8b). This fraction is almost the same for all sizes: it reflects the size-invariance of the collisional process imposed by both

(i) the assumed exponent of the size-distribution, and
(ii) the use of a size-independent impact strength (S).

The exponent of the resulting size-distribution has decreased from -3.6 to -3.5 in about 10^4 years. The mass contained in bodies larger than 1 km, $M(> 1\ \text{km})$, is shown in Fig. 8c as a function of time. Because of the high initial collision rate (see Section 3.2), $M(> 1\ \text{km})$ decreases first very rapidly, with a 2×10^4 year timescale. However this period lasts only for 1000 years due to the rapid depletion of the disk. As a consequence $M(> 1\ \text{km})$ decreases more and more slowly and stabilizes at about $8 - 9 M_\oplus$ after 4×10^4 years. It seems to continue to decrease on a much longer timescale. A linear extrapolation suggests that another few 10^6 years may be required for $M(> 1\ \text{km})$ to decrease by another factor

of 2. However, the real timescale may be orders of magnitudes longer due to the rapid dynamical depletion of the disk: for example, Holman and Wisdom (1993) find that all particles initially in the Jupiter–Saturn region suffer a close encounter with the giant-planets in 10^6 years after which they are rapidly scattered away from the Jupiter–Saturn region. Thus, it is probable that the distribution of planetesimals is frozen after only a few 10^4 years of evolution. Only some of the remaining bodies are pristine (see Fig. 8c). The number of pristine planetesimals increases steeply with mass. Notice that although only 30% of kilometer sized bodies survived the collisional process intact, 70–100% of bodies larger than 10 km are pristine.

Increasing the mass of the biggest planetesimals from 50 to 500 km at constant total mass (and keeping $q = -3.6$), substantially modifies the previous results because of the smaller number of small bodies. As a result the collisional evolution is much slower compared to the previous case. To illustrate this, the distribution C1-2 is considered here with $R_{max} = 500$ km but the same power law slope ($q = -3.6$) and the same total mass ($11.5M_\oplus$). Results are shown with bold dashed-line in Fig. 8. At the end of the run, the size distribution is almost unaltered: 85 to 100% of the original number of bodies in each mass bin survive (Fig. 8b). Among these bodies, 80 to 100% of bodies larger than 10 km are pristine, as are 50% of the kilometer sized bodies.

Broken power-law size-distributions are now considered: distributions C2-1 and C2-2 of Table 2, characterized by a size of the biggest bodies equal to 50 and 500 km in radius, respectively. In both cases, the mass is contained mostly in the small bodies. As a consequence, the mass of the largest bodies is a parameter that has little influence on the evolution of the size distribution, so that the two cases can be barely distinguished in Fig. 8 (thin solid and dashed lines). Only 20% of the initial number of bodies smaller than 1 km (in the fragmentation tail $q \sim -3.5$) remains at the end of the run (Fig. 8b). In the accretion tail ($q \sim -5.5$) the fraction of remaining bodies increases steeply with size from 20% for 1 km bodies to 80% and more for 50–500 km bodies. This slope reflects the tendency for the size-distribution to converge toward a -3.5 power law slope. At the end of the run $q \simeq -5.1$ for bodies $\geqslant 1$ km. Thus the ratio of the final to the initial size-distribution behaves as $r^{5.5-5.1=0.4}$. The remaining mass $M(> 1$ km$)$ is about $1/5$ of its starting value, reflecting mainly the evolution of kilometer-sized bodies which dominate the cumulative mass of bodies larger than 1 kilometer. The fraction of remaining pristine bodies is very different from previous cases (Fig. 8d), with a clear transition at 1 km radius. Below 1 km, the slope is comparable to other previous cases, but the limit of 50% survivors is around 500 m rather than in the 1–10 km range (for cases C1-1 and C2-2). Whereas sub-kilometer sized bodies are almost all fragments, bodies larger than 1 km are mainly pristine ($> 80\%$). This very different behavior in the accretion tail ($r > 1$ km) comes from the -3 to -4 power law exponent of the fragment distribution, which is shallower than the

-5.5 power law of the original size-distribution. Fragments with $dn/dr \propto r^{-3-4}$ are added to a pristine population distributed with $dn/dr \propto r^{-5.5}$. As a simple numerical result, fragments are far less numerous compared to the number of pristine bodies. The large fraction of surviving bodies in the accretion tail simply reflects this mechanism.

3.3.2. A high and low total mass ($50M_\oplus$ and $6.6M_\oplus$)

The total mass of planetesimals may be an important factor since the greater the mass, the greater the collision rate and the faster the collisional evolution. For the same sizes distribution, the collision frequency is expected to vary linearly with the total mass. We turn to cases C1-3 ($q = -3.6$, $R_{max} = 50$ km) and C1-4 ($q = -3.6$, $R_{max} = 500$ km) containing $50M_\oplus$ of planetesimals between Jupiter and Saturn (5 times the minimum mass nebula). Results are summarized in Table 2. Destruction is indeed more rapid than for the $11.5M_\oplus$ case, but final results are still comparable to our standard case: The ratio of the final to the initial mass in bodies larger than 1 km is 50% to 83% (compared to 75% and 93% for the standard case). Evolutions of bimodal distributions C2-3 ($R_{max} = 50$ km) and C2-4 ($R_{max} = 500$ km), are again very similar to the $11.5M_\oplus$ case. We now turn to the case of a smaller initial mass, considering $6.6M_\oplus$ of solid material between Jupiter and Saturn (0.6 times the minimum-mass nebula). For all initial distributions considered here (C1-5, C1-6, C2-5, C2-6), the qualitative results are again similar to the $11.5M_\oplus$ case, but with a somewhat longer destruction timescale. For single power-law distributions with $q = -3.6$ (C1-5 and C1-6) the mass-fraction of surviving bodies of 1 km is about 80%, whereas for the bimodal size-distributions C2-5 and C2-6) it is around 30%, rising up to more than 55% for bodies larger than 10 km. In conclusion, it seems that the total mass of solid-material moderately influences the fraction of surviving planetesimals.

3.3.3. Weaker bodies ($S = 10^5$ erg/cm^3)

In the previously discussed simulations bodies with impact strength $S = 3 \times 10^6$ erg/cm^3 were considered. Since planetesimals are suspected to be very weak bodies, new simulations were run, corresponding to the standard case (distributions C1-1, C1-2, C2-1, C2-2), but with impact strength decreased to $S = 10^5$ erg/cm^3, thirty times smaller than previously assumed. The evolution of weaker planetesimals is displayed in Fig. 9 and may be compared to Fig. 8. The mass remaining in bodies larger than 1 km at the end of the run (Fig. 9c) is $3M_\oplus$ and $8M_\oplus$ for distributions C3-1 and C3-2, respectively, compared to 8 and $10.5M_\oplus$ for the standard case. For distributions C3-1 and C3-2, $M(> 1$ km$)$ is about $0.75M_\oplus$ at the end of the run compared to $1M_\oplus$ for the standard case, reflecting mainly the destruction of the smallest bodies. The limit of 50% survivors is around 50–100 m. Thus, erosion is indeed more efficient than for the $11.5M_\oplus$ case, but the mass of remaining material is not low-
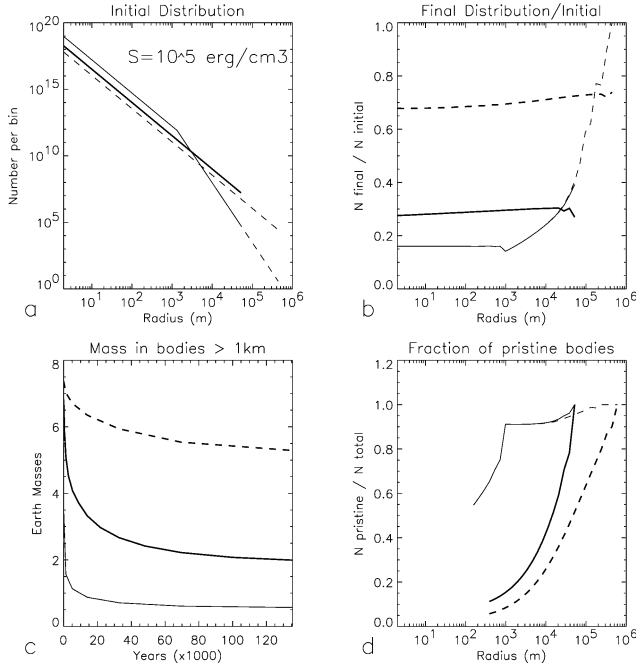
Fig. 9. The total mass of planetesimals is $11.5M_\oplus$ and the material strength is lowered to 10^5 erg/cm³. Evolution for initial size-distribution C4-1 (bold solid), C4-2 (bold dash), C4-3 (solid), C4-4 (dashed) (see Table 2 for description). See caption of Fig. 8 for details.

Fig. 10. The total mass of planetesimals is $11.5M_\oplus$ and the material strength is scaled according to a strain-rate model (Housen et al., 1991). Evolution for initial size-distribution C1-1 (bold solid), C1-2 (bold dash), C2-1 (solid), C2-2 (dashed) (see Table 2 for description). See caption of Fig. 8 for details.

ered by orders of magnitude (as inferred in previous studies), but rather by a factor of 2 compared to our standard case.

3.3.4. Size-dependent impact-strength

A size-dependent S implies a size-dependent fragmentation process. Strictly speaking, the recipe adopted for the elimination of the cut-off effect at smaller sizes (Section 2.3.2) becomes inconsistent. However, results should be roughly correct for kilometer-sized bodies and larger, because the collisional evolution is self-consistently computed down to meter-sized bodies. We first consider the popular strain-rate scaling law of Housen et al. (1991) for the impact-strength, scaled to 3×10^6 erg/cm³ for 10 cm bodies (Ryan et al., 1991, 1999, see Fig. 2). The weakest bodies are in the range 1 to 10 km, with S about 5×10^5 erg/cm³. Because of their low impact-strength, these bodies are rapidly collisionally destroyed. Results are displayed in Fig. 10, in the standard case (a $11.5M_\oplus$ disk) with the four usual starting size distributions (referred to as C4-1 to C4-4 in Table 2). For all cases considered here, kilometer-sized planetesimals disappear in priority: only 15% to 45% survive depending on the initial distribution. It is significantly smaller than previous cases with a constant $S = 10^6$ erg/cm³. Note that half of the kilometer-sized planetesimals disappear in ~ 6000 years, in rough agreement with SW01, who also used a strain-rate scaling law model. However, the fraction of surviving planetesimals is almost constant after 10^4 years. Moreover, quite different results are found when using a recent scaling law for icy bodies hit by projectiles at 3 km/s obtained with a 3D SPH hydrocode model (Benz and Asphaug, 1999). This law
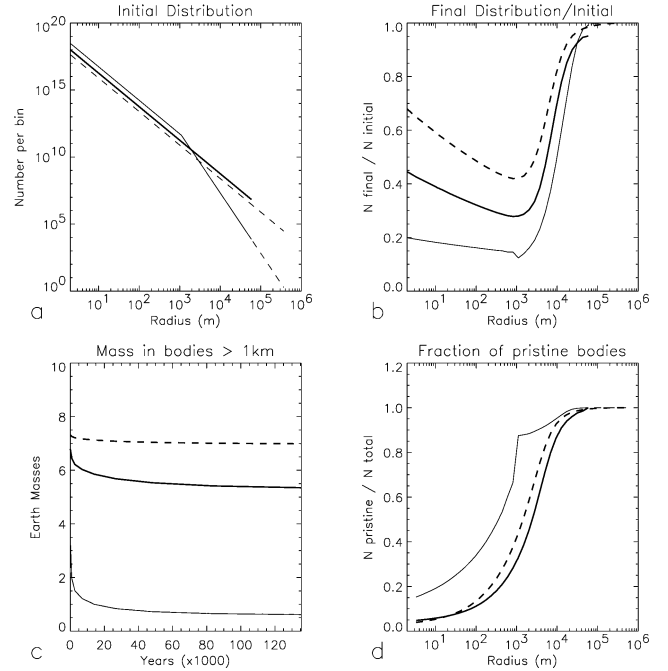
is presented in Fig. 2. The weakest bodies are in the range 100 m, the gravitational regime beginning at 1 km. The corresponding evolution of planetesimals is shown in Fig. 11. The ratio of the final to the initial size distribution shows clearly a gap around 100 m bodies, reflecting a faster collisional evolution of the weakest bodies. The final number of kilometer-sized bodies is high: from 30 to 80% of the initial distribution survives, depending on the initial size distribution. This comes partly from the rapid depletion of the 100 m planetesimals, which become too few to efficiently destroy larger bodies. As a result, only little decrease of $M(> 1\ km)$ is observed (Fig. 11c).

3.4. A first insight into collisional damping

One important aspect that our model cannot treat is the effect of collisional damping. Indeed one may wonder if collisions may efficiently damp eccentricities and inclinations so that planetesimals are "stuck" in the giant planet region for a long time-period, up to the epoch when the mass has sufficiently decreased. This point was first raised by SW01. For collisional damping to be efficient, the typical collision timescale may be comparable, or even lower, than the typical ejection timescale induced by giant planets. Let us consider the simple case of a $11.5M_\oplus$ disk made of 1 km bodies. The collision-time in absence of perturbations is $T_{coll} \sim 5 \times 10^4$ years and goes down to $T_{coll} \sim 8 \times 10^3$ years after 100 years (see Fig. 4), after which it increases again. The timescale for the dynamical excitation (T_{exc}) is about 2×10^4 years.
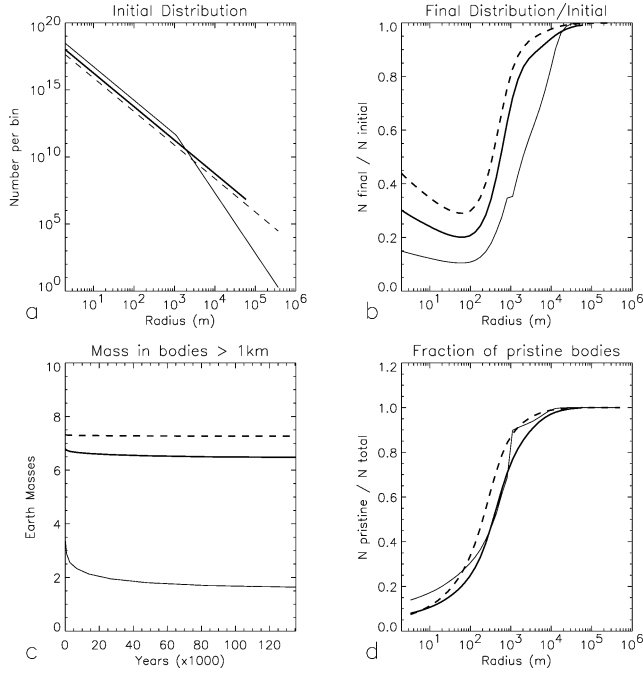
Fig. 11. The total mass of planetesimals is $11.5 M_\oplus$ and the material strength is scaled according to the 3D hydrocode model of Benz and Asphaug (1999). Evolution for initial size-distribution C1-1 (bold solid), C1-2 (bold dash), C2-1 (solid), C2-2 (dashed) (see Table 2 for description). See caption of Fig. 8 for details.

Fig. 12. Eccentricity versus semi-major axis after 3×10^5 years of evolution for particles that did not suffer any collision (left) and for particles that suffered at least 1 collision (right).

Since at any time, $T_{coll} \geqslant T_{exc}$ one may expect collisional damping to be inefficient. Astrophysical systems with efficient collisional damping are very few (apart from the case of fluid-systems, which are completely dominated by collisions). For example, planetary rings are subject to a strong damping, especially in Saturn's B ring, but the collision rate is a few tens of collisions per orbital period, and gravitational stirring induced by satellites is much weaker than those induced by Jupiter and Saturn. To go beyond these simple considerations, a simple numerical model was run, which is described in detail in Charnoz et al. (2001). It is a disk made of 5000 equal and finite-size particles suffering hard-spheres inelastic collisions and gravitational perturbations from Jupiter and Saturn. The particle's radius is scaled such that the collision rate in the numerical simulation is the same as in a quiet planetesimal disk extending from Jupiter to Saturn. As shown in Trulsen (1971), Brahic (1976), and illustrated in Charnoz et al. (2001) the collisional evolution of a system made of a large number of small particles may be simulated with a small number of large particles if the collision rate is the same in both systems. As particles cross each other, they suffer inelastic rebounds as described in Brahic (1976), with a constant radial restitution coefficient of 0. So, there is on average, 50% energy dissipation over all directions. In such a model, fragmentation cannot be taken into account self-consistently as well as the particles' size-distribution because of the small number of particles. However, we still think that the results may give us a first insight into the question of collisional damping.
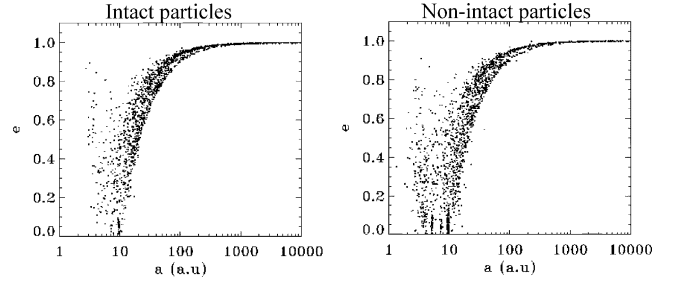
Initial conditions are chosen to reproduce the collision-rate of a disk made of kilometer-sized planetesimals with total mass consistent with the minimum mass solar nebula, in addition to the mass of the giant planets. In order to do this with only 5000 particles, the particle radius must be of 5×10^{-4} AU. The simulation was performed during 3×10^5 years of evolution (three times longer than for the previous model). Results are shown in Fig. 12. Over the 5000 initial particles, 1561 were ejected from the system ($e > 1$), with 55% of them having suffered at least one collision (and 45% have not suffered collision). Of the remaining particles ($e < 1$), 1832 suffered at least one collision, which represents 53% of them (and 47% of intact particles). Despite dissipation in inelastic collisions the large majority of both intact and non-intact particles remaining in the system is transported to greater heliocentric distances, indicating that particles are not retained by collisions in the Jupiter–Saturn region. Most particles located in the Lagrangian-points of Jupiter and Saturn have suffered collisions; however, a comparison with a collision-less simulation shows that their dynamics is very similar to the collisional case. In conclusion, Fig. 12 shows that there is little difference between the global dynamics of intact particles and the dynamics of particles that suffered collisions. This suggests that collisional damping is inefficient. Non-intact particles are somewhat more widely spread at smaller heliocentric distances. This simple model does not give the final answer to the question of collisional damping (the use of a single particle size may result in an underestimate of the real collisional activity induced by bodies of different sizes but, unfortunately, computer limitations do not allow us to do better), but it strongly suggests that collisions do not modify the global dynamics of the system, and supports the dynamical studies of the Oort cloud formation which did not include collisions (as in Duncan et al., 1987; see Weissman, 1996, for a review).

4. Conclusions

We have presented a new approach designed to track the collisional evolution of a population of small bodies evolving under strong gravitational perturbations, such as those exerted by giant planets. Our approach is superior to the clas-

sical Particle-In-A-Box approach, because it starts from a realistic representation of the dynamics given by a *N*-body code, and accounts for the feedback of the dynamical evolution onto the collisional evolution. As an example of application, and to stress the differences of the results with respect to those of the classical approach, we study the evolution of the size-distribution of planetesimals during their ejection towards the Oort cloud caused by the scattering action of the giant planets. As a first approach, this work is restricted to the Jupiter–Saturn region, where collisional and dynamical timescales are shorter compared to the Uranus and Neptune regions because of

(1) a high density of planetesimals,
(2) a small heliocentric distance; and
(3) the large masses of the perturbing planets.

Our main goal has been to quantify which fraction of planetesimals is destroyed in catastrophic collisions before that they can reach the Oort cloud. Concerning the sole dynamics of the ejection induced by Jupiter and Saturn, we find that:

1. Bodies between Jupiter and Saturn are efficiently transported away and the number of planetesimals within the orbit of Saturn is halved in less than 5×10^4 years, in good agreement with previous studies (Holman and Wisdom, 1993).
2. Particle inclinations are raised less rapidly than eccentricities in the first 1000 years of evolution due to the small inclinations of Jupiter and Saturn (with respect to the invariable plane). As a consequence of the high e/i ratio ($\gg 2$), the collision times falls strongly in the first 10^3 years: from 1 collision/particle every 5×10^4 years to 1 collision/particle every 5×10^3 years (Fig. 4) for a standard $10 M_\oplus$ population composed of kilometer-sized planetesimals between Jupiter and Saturn.
3. After 10^3 years evolution, the collision time again increases monotonically due to the progressive excitation of the inclinations and the dynamical depletion of the disk.
4. Collisions are preferentially located
   (1) at Jupiter's and Saturn's orbit (because bodies in the 1 : 1 resonance with a planet are stable and offer a cumulatively large collision cross-section and also because scattered bodies keep their perihelia locked close to the giant planet's orbit); and
   (2) between 6 and 8 AU, a region in which the ejection timescale is longer than close to the giant planets (Holman and Wisdom, 1993).

Following this dynamical study, the evolution of the size-distribution for several starting population was considered, varying parameters like the total mass, the largest body's mass and for material strength. Our results are summarized in Table 2. Our main results are the following:

1. In all cases, the rapid dynamical depletion of the disk allows a substantial fraction of the total mass of planetesimals to survive in bodies larger than 1 km (either pristine or fragments). In the manner of a hot gas which expands violently, the collision rate falls dramatically after $\sim 10^4$ years as the disk is progressively blown-out. As a result, the system is "frozen" after $1–2 \times 10^4$ years evolution. The fractional surviving mass depends strongly on the initial total mass, the size-distribution and the material strength. Over all cases considered here, 15 to 90% of the mass contained in bodies larger than 1 km remains in bodies larger than 1 km. This fraction grows to 25–100% for bodies larger than 10 km. For the standard case (twice the minimum mass nebula including Jupiter and Saturn's mass, $S = 3 \times 10^6$ erg/cm^3, power-law size-distribution), more than 70% of the mass in bodies larger than 1km remains in this form at the end of the run. Note that this ratio falls down to 22% if the initial size-distribution is a broken power law with a break at 1 km.
2. For the same total mass of planetesimals, the larger the biggest body, the slower the collisional evolution. If 500 to 1000 km bodies were initially present between Jupiter and Saturn, more than 50% of the mass contained in bodies larger than 10 km remains at the end of the evolution in all cases encountered here.
3. An impact-strength varying with size was also considered, and the result depends substantially on the chosen scaling law. Two laws were considered here (an analytical strain-rate model and a recent law coming from a 3D-hydrocode), for which weakest bodies are respectively ~ 1 km or ~ 100 m. In the first case, the destruction of km-sized bodies is at first very rapid, but at least 15% of them survive in all cases considered, thanks to the dynamical depletion of the disk. For the recent hydrocode scaling-law, up to 75% of kilometer-sized bodies survive when the initial size-distribution has a slope at collisional equilibrium (~ 3.5). Bodies larger than, respectively, 10 and 1 km easily survive due to their self-gravity.
4. The size limit for having at least 50% pristine bodies (or survivors) is in the range 100 m to 10 km depending on the choice of the parameters (see Table 2). For a broken power-law size-distribution, bodies in the steep part of the distribution are almost all pristine. Because of the wide range of parameters the results have a correspondingly wide range. Note that for our standard case, 25 to 100% of bodies larger than 1 km are pristine at the end of the run. In the case of an initial distribution with a biggest body of 500 km, the fraction of pristine bodies larger than 1 km is in the range 50 to 100%. The most favorable case is for bi-modal initial-distributions for which the fraction of pristine bodies is always larger than 80% for bodies larger than the transition radius (1 km here).

By using a direct simulation employing finite-size particles suffering dissipative hard-sphere collisions, we also investigated if collisions can damp eccentricities and inclinations and prevent planetesimals from being ejected towards the Oort cloud. Despite the simplicity of the adopted model, our results suggest that the global dynamics is not substantially modified by collisions and that most particles are ejected to the outer Solar System despite collisions.

This work echoes that of SW01 because, from a qualitative point of view, we also find that planetesimals suffer a rapid collisional evolution at the very beginning of their gravitational scattering by Jupiter and Saturn. However, from a quantitative point of view, the use of our new approach, which couples collisions and dynamics, reveals that the erosion process is less efficient than suggested by SW01. In SW01, only 0.1 to 10% of the bodies larger than 1 km in the Jupiter–Saturn region survive the collisional grinding and are ejected towards the Oort cloud. In our calculations, the corresponding fraction ranges from 15 to 95%, depending on the parameters used in the simulation. These differences show the importance of following a more sophisticated approach like the one that we have developed, rather than a classical Particle-In-A-Box approach as in SW01. The differences in the results are in fact entirely due to the different computational approach. Indeed we are able to recover SW01 results if we artificially suppress the dynamical scattering of the planetesimals by the giant planets (the typical destruction timescale we find is about 6000 years for strong material, close to 4000 years found by SW01).

For what concerns the problem of the origin of the Oort cloud, our results suggest that the conclusions of SW01 should be tempered and reabilitates the classical collisionless model of the formation of the Oort cloud by gravitational scattering, as described in Duncan et al. (1987). Our conclusion on the insubstantial role of collisions is strictly valid only for the Jupiter–Saturn region, which is well known to have only a minor role in the formation of the Oort cloud for dynamical reasons. For a more appropriate study of the role of collisions in the Oort cloud formation process, in a future paper we will extend our analysis to the entire giant-planet region, up to the Kuiper belt. We stress that our computational approach is suitable for a variety of interesting problems, such as the collisional evolution of the Kuiper belt, the asteroid belt and of the population of the irregular satellites of the giant planets, during the primordial sculpting of the Solar System.

Acknowledgments

References

Benz, W., Asphaug, E., 1999. Catastrophic disruptions revisited. Icarus 142, 5–20.

Brahic, A., 1976. Numerical simulation of a system of colliding bodies in a gravitational field. J. Comp. Phys. 22, 171–188.

Campo-Bagatin, A., Cellino, A., Davis, D.R., Paolicchi, P., 1994. Wavy size-distributions for collisional systems with a small-size cutoff. Planet. Space Sci. 42, 1079–1092.

Charnoz, S., Thébault, P., Brahic, A., 2001. Short-term collisional evolution of a disk perturbed by a giant-planet embryo. Astron. Astrophys. 373, 683–701.

Colwell, J., Esposito, L.W., Bundy, D., 2000. Fragmentation rates of small satelites in the outer Solar System. J. Geophys. Res. 105 (E7), 17589–17600.

Davis, D.R., Farinella, P., Paolicchi, P., Weidenschilling, S.J., Binzel, R.P., 1989. Asteroid collisional history—effects on sizes and spins. In: Binzel, R.P., Gehrels, T., Matthews, M.S. (Eds.), Asteroids II. Univ. of Arizona Press, Tucson, pp. 805–826.

Davis, D.R., Farinella, P., 1997. Collisional evolution of Edgeworth–Kuiper belt objects. Icarus 125, 50–60.

Dohnanyi, J.W., 1969. Collisional model of asteroids and their debris. J. Geophys. Res. 74, 2531–2554.

Duncan, M., Quinn, T., Tremaine, S., 1987. The formation and extent of the Solar System comet cloud. Astron. J. 94, 1330–1338.

Fujiwara, A., Kamimoto, G., Tsukamoto, A., 1977. Destruction of basaltic bodies by high-velocity impact. Icarus 31, 277–288.

Greenberg, J.M., Wacker, J.F., Hartmann, W.L., Chapman, C.R., 1978. Planetesimals to planets—numerical simulation of collisional evolution. Icarus 35, 1–26.

Hertzsch, J.-M., Scholl, H., Spahn, F., Katzorke, I., 1997. Simulation of collisions in planetary rings. Astron. Astrophys. 320, 319–324.

Holman, M.J., Wisdom, J., 1993. Dynamical stability in the outer Solar System and the delivery of short period comets. Astron. J. 105, 1987–1999.

Housen, K.R., Schmidt, R.M., Holsapple, K.A., 1991. Laboratory simulations of large-scale fragmentation events. Icarus 94, 180–190.

Kenyon, S.J., Luu, J.X., 1999. Accretion in the early outer Solar System. Astron. J. 118, 1101–1119.

Marzari, F., Davis, D., Vanzani, V., 1995. Collisional evolution of asteroid families. Icarus 113, 168–187.

Marzari, F., Farinella, P., Davis, D.R., Scholl, H., Campo-Bagatin, A., 1997. Collisional evolution of trojan asteroids. Icarus 125, 39–49.

Nobili, A.M., Milani, A., Carpino, M., 1989. Fundamental frequencies and small divisors in the orbits of the outer planets. Astron. Astrophys. 210, 313–336.

Paolicchi, P., 1994. A semiempirical model of catastrophic breakup processes. Planet. Space Sci. 42, 1093–1097.

Petit, J.-M., Farinella, P., 1993. Modelling the outcomes of high-velocity impacts between small Solar System bodies. Celest. Mech. Dyn. Astr. 57, 1–28.

Ryan, E.V., Hatrmann, W.K., Davis, D.R., 1991. Impact experiments. III. Catastrophic fragmentation of aggregate targets and relation to asteroids. Icarus 94, 283–298.

Ryan, E.V., Davis, D.R., Gibliin, I., 1999. A laboratory impact study of simulated Edgeworth–Kuiper belt objects. Icarus 142, 56–62.

Spaute, D., Weidenschilling, S.J., Davis, D.R., Marzari, F., 1991. Accretional evolution of a planetesimal swarm. I. A new simulation. Icarus 92, 147–164.

Stern, S.A., Colwell, J.E., 1997. Collisional erosion in the primordial Edgeworth–Kuiper belt and the generation of the 30–50 Au Kuiper gap. Astron. J. 490, 879–884.

Stern, S.A., 1991. On the number of planets in the outer Solar System—evidence of a substantial population of 1000-km bodies. Icarus 90, 271–281.

Stern, S.A., Weissman, P.R., 2001. Rapid collisional evolution of comets during the formation of the Oort cloud. Nature 409, 589.

Tanaka, H., Inaba, S., Nakazawa, K., 1996. Steady-state size distribution for the self-similar collision cascade. Icarus 123, 450–455.

Trulsen, J., 1971. Toward a theory of jet streams. AP&SS 12, 239.

Weissman, P.R., 1996. The Oort cloud. In: Rettig, T.W., Hahn, J.M. (Eds.), Completing the Inventory of the Solar System. In: ASP Conf. Ser., Vol. 107. Astronomical Society of the Pacific, San Francisco, pp. 265–288.

Wetherill, G.W., 1967. Collisions in the asteroid belt. J. Geophys. Res. 72, 2429–2444.

Wetherill, G.W., Stewart, G.R., 1989. Accumulation of a swarm of small planetesimals. Icarus 77, 330–357.

Wetherill, G.W., Stewart, G.R., 1993. Formation of planetary embryos—effects of fragmentation, low relative velocity, and independent variation of eccentricity and inclination. Icarus 106, 190–209.